

# Complex Human Hair Bearing Skin Organoids as Model for Herpes Simplex Virus 1 Infection in the Skin

Emanuel Wyler<sup>\*1</sup>, Silvia Albertini<sup>\*2</sup>, Caroline C. Friedel<sup>3</sup>, Artür Manukyan<sup>1</sup>, Jiabin Huang<sup>4</sup>, Susanne Krasemann<sup>5</sup>, Izabela Plumbom<sup>6,7</sup>, Janine Altmüller<sup>6,7</sup>, Thomas Conrad<sup>6,7</sup>, Helena Radbruch<sup>8</sup>, Wali Hafezi<sup>9</sup>, Arne Hansen<sup>10</sup>, Adam Grundhoff<sup>11</sup>, Markus Landthaler<sup>1,12</sup>, Nicole Fischer<sup>2</sup>, Manja Czech-Sioli<sup>4#</sup>

<sup>1</sup> Max Delbrück Center for Molecular Medicine in the Helmholtz Association (MDC), Berlin Institute for Medical Systems Biology, Berlin, Germany

<sup>2</sup> Institute for Molecular Virology and Tumovirology, University Medical Center Hamburg-Eppendorf Hamburg, Germany

<sup>3</sup> Institute for Informatics, Ludwig-Maximilians-Universität München, Munich, Germany

<sup>4</sup> Institute of Medical Microbiology, Virology and Hygiene, University Medical Center Hamburg-Eppendorf Hamburg, Germany

<sup>5</sup> Institute of Neuropathology, University Medical Center Hamburg-Eppendorf, Hamburg, Germany

<sup>6</sup> Genomics Technology Platform, Max Delbrück Center for Molecular Medicine in the Helmholtz Association, Berlin, Germany

<sup>7</sup> Core Facility Genomics, Berlin Institute of Health at Charité - Universitätsmedizin Berlin, Berlin, Germany

<sup>8</sup> Department of Neuropathology, Charité – Universitätsmedizin Berlin, Berlin, Germany

<sup>9</sup> University Hospital Muenster, Institute of Virology / Clinical Virology, Muenster, Germany

<sup>10</sup> Institute of Experimental Pharmacology and Toxicology, University Medical Center Hamburg-Eppendorf, Hamburg, Germany

<sup>11</sup> Leibniz Institute of Virology, Hamburg, Germany.

<sup>12</sup> Institut für Biologie, Humboldt-Universität zu Berlin, Berlin, Germany

\* These authors contributed equally

# To whom correspondence should be addressed: [m.czech-sioli@uke.de](mailto:m.czech-sioli@uke.de)

## Abstract

For Herpes Simplex Virus 1 (HSV-1) the skin is the primary site of infection. After the primary lytic infection, the virus enters the peripheral nervous system where it establishes latency. Spontaneous reactivation from the latently infected neurons leads to the typical HSV-1-induced diseases like cold sores. Modelling HSV-1-induced skin pathologies is challenging due to the variety of different cell types and structures in the skin and human-specific responses to the infection. Nevertheless, studies using monolayer cell lines, raft cultures, *ex vivo* skin and mouse models provided an immense contribution to our understanding of HSV-1 infection in the skin. However, the contribution of many skin-specific structures, especially hair follicles, to primary infection and reactivation remains unclear. In this study, we used complex human hair bearing skin organoids that were derived from induced pluripotent stem cell as a model for HSV-1 infection. We performed microscopy, bulk and spatial transcriptomics with single cell resolution to gain new insights into the cell-type specific viral life cycle and host responses. We show a restricted viral infection in keratinocytes of the epidermis and specific cell types of hair follicles. We show a cell type specific induction of interferon-stimulated genes and the TNF pathway. We can follow paracrine signaling through the tissue, showing that TNF response genes are upregulated in adjacent cells. Taken together, the skin organoids in combination with novel spatial transcriptomics techniques provide a physiologically highly relevant model system for HSV-1 infection in the skin.

## Introduction

Herpes Simplex Virus 1 (HSV-1) is a highly prevalent human pathogen with a global prevalence of ~67% in under 50-year-old individuals<sup>1</sup>. Primary infection usually occurs via the mucosal surfaces or micro-lesions in the skin. Initially HSV-1 productively replicates in the epithelial cells of skin and mucosa causing inflammation and tissue damage and consequently blisters<sup>2</sup>. After replication in epithelial cells, HSV-1 enters the nerve endings of peripheral neurons and travels along their axons to the cell bodies in trigeminal ganglia where it establishes latency<sup>3,4</sup>. Upon spontaneous reactivation, HSV-1 enters the lytic life cycle and produces infectious viral particles that travel along the axons in an anterograde manner to the epithelial cells of skin and mucosa. The following lytic replication in the epithelium leads to the characteristic herpes lesions that release virus to the environment<sup>2</sup>.

In the past, many different model systems have been used to elucidate the mechanisms of primary infection and reactivation by HSV-1 in the skin. Due to the complexity of skin and the involvement of many different cell types, *in vitro* modelling by monolayer cell cultures can only recapitulate certain aspects of the viral life cycle. More complex model systems used to study virus susceptibility, spread and cytopathic effects are animal models<sup>5-8</sup>, *ex vivo* murine<sup>8-10</sup> and human skin explants<sup>8,11,12</sup>, and epithelial raft cultures<sup>13,14</sup>.

While the understanding of HSV-1 pathogenesis in the skin has exceptionally increased using these model systems, many aspects remain elusive. Especially the susceptibility and contributions of specific structures, like hair follicles, different fibroblasts subpopulations and low abundance cell types, to primary infection, latency establishment and reactivation are not understood. The field of organoids is constantly evolving and creating potential new model systems for virus research<sup>15-17</sup>. In this study we used a highly complex skin organoid (SkO) model generated from human induced pluripotent stem cells (hiPSCs) for the analysis of HSV-1 pathogenesis in the skin. The SkOs were generated after a protocol from Lee and colleagues<sup>18,19</sup>. They contain a stratified epidermis, fat-rich dermis, pigmented hair producing hair follicles, sebaceous glands, melanocytes and Merkel cells. The hair follicles are innervated by sensory neurons that are covered in Schwann cells on their axons while their somata assemble in trigeminal like clusters together with satellite glial cells. SkOs contain all cell types expected in the fetal skin of the second trimester of development except for sweat glands, vascularization and immune cells<sup>18,19</sup>. Similar to many other organoids, SkOs show an inside out morphology with the dermis being exterior and exposed to the culture medium and the epidermis being interior with hair from hair follicles growing to the inside of the organoid. In our study, we infected SkOs with HSV-1 from the dermal site, leading to infection of the dermal fibroblasts first and then the keratinocytes therefore mimicking a primary infection by deep wounding inside the dermis or by reactivation. By using microscopy, bulk and spatial transcriptomics, we reveal how HSV-1 spreads in the tissue and analyze the spatial and temporal host response.

## Material and Methods

### SkO generation and microscopy

SkOs were generated from the human iPS cell line UKEi001-A according to the protocol by Lee and colleagues<sup>19</sup>. All procedures involving the hiPSC lines were approved by the local ethics committee in Hamburg (Az PV4798, 28.10.2014). Only SkOs showing correct differentiation as determined by the appearance of hair follicles (HF) at 110 to 120 days post production were used for further experiments.

For immunohistochemistry SkOs were fixed in 4% buffered formalin over night at 4°C and then transferred to PBS. Afterwards they were protected in 3% agarose, dehydrated using a Leica ASP300S tissue processor, and embedded in paraffin. Organoid paraffin sections were cut at 3 µm and stained with hematoxylin and eosin (H&E) according to standard procedures. For immunohistochemical staining sections (3 µm) were processed as following: After dewaxing

and inactivation of endogenous peroxidases (3% hydrogen peroxide), antibody specific antigen retrieval was performed using the Ventana BenchMark XT autostainer (Ventana, Tuscon, Arizona, USA). Sections were blocked and afterwards incubated with the primary antibodies, see Table S1. For detection of specific binding and DAB staining, the UltraView Universal DAB Detection Kit (Roche, #760-500) was used, which contains both, anti-mouse and anti-rabbit secondary antibody. Counter staining and bluing were performed with Hematoxylin (Ventana Roche, # 760-2021) and Bluing Reagent (Ventana Roche, # 760-2037) for 4 min. Subsequently, stained sections were mounted in mounting medium.

For immunofluorescence staining, paraffin organoid sections were cut at 3  $\mu$ m and thoroughly deparaffinized in 2x 20 minutes in Xylene and a descending alcohol row. Antigen retrieval was then performed by pressure boiling the sections in Universal R buffer (#AP0530-500; Aptum, UK) for 20 minutes (2100 Antigen Retriever; Aptum). Sections were briefly rinsed and blocked for 1 hour (MAXblock, Active Motif). Antibodies (see Table S1) were incubated overnight at 4°C. After intensive washing, AlexaFluor488-, AlexaFluor555, or AlexaFluor647-coupled secondary antibodies were applied for 1.5 hours. Sections were washed again, counterstained with DAPI and mounted in Fluoromount-G (SouthernBiotech, Birmingham, USA).

Pictures of IHC and immunofluorescence staining were acquired with the Sysmex Panoramic MIDI II slide scanner. Image cropping was performed with QuPath0.4.3 and pictures assembled with Microsoft PowerPoint.

For whole mount staining of SkOs the qCe3D method was used according to Lee and colleagues<sup>19</sup> with the following adjustments: Clearing was performed for 48hrs and stained and cleared SkOs were mounted in iSpacer (SUNJinLab) 4 well imaging spacers. For antibodies see Table S1. Imaging was performed with a Leica TCS SP8 X confocal microscope. Images were processed with Imaris and ImageJ 2.14 and pictures assembled with Microsoft PowerPoint.

## Virus infection

HSV-1 17 CMV-IEproEGFP expressing EGFP under the control of the CMV IE promoter was described before<sup>20</sup>. The virus was propagated on Vero cells and the infection titer determined by plaque assay. Before infection the medium on SkO was exchanged and again 12hrs after infection. Afterwards medium exchange was performed every day.

## Bulk RNA-seq

For bulk RNA-seq 4 SkOs per condition (untreated, 2 days post infection (dpi), 4 dpi, 6 dpi, 8 dpi) were used. Total RNA was isolated individually from each SkO by adding QIAzol lysis reagent (Qiagen) and disrupting the organoid by grinding with a pestle. The lysate was homogenized with a QIAshredder (Qiagen). After one round of chloroform extraction, RNA was cleaned up with the RNeasy MinElute Cleanup Kit (Qiagen). DNA was two times digested with the DNA-free DNA removal kit (Thermo Fisher Scientific). RNA concentration was determined with the Qubit RNA broad range assay (Thermo Fisher Scientific) and equal amounts of RNA from two SkO of the same condition were pooled resulting in duplicates for each condition for sequencing. RNA integrity was determined via a Bioanalyzer RNA 6000 Pico Assay (Agilent, 5067-1514). RIN values were in the range between 5.5 and 9.2. From each sample 520 ng total RNA was subjected to rRNA depletion (following the Lexogen RiboCop rRNA Depletion Kit for Human/Mouse/Rat V2 protocol, catalog number: 144.24) and further processed via the RNA-Seq V2 Library Prep Kit with UDIs (Lexogen, catalog number: 175.96) in the short insert size variant (RTM) according to manufacturer's instructions. Libraries were quality controlled on a Bioanalyzer High Sensitivity DNA Assay (Agilent, 5067-4626) and were sequenced on an Illumina NextSeq 500 instrument with NextSeq 500/550 High Output Kit v2.5 (75 Cycles, product number: 20024906) in a single-read mode (1 x 83 bp). After demultiplexing via bcl2fastq, 20.7 – 28.6 million (M) read pairs assigned to each sample. All samples passed

quality control by fastqc and were subjected to downstream analysis. Processing was done with the nf-core/RNA-seq pipeline (v3.12.0) within the nf-core framework<sup>21</sup>. The pipeline was executed with Nextflow v23.04.1<sup>22</sup>, utilizing STAR (v2.6.1d)<sup>23</sup> for alignment to the GRCh38 human genome and Human herpesvirus 1 genome (X14112.1), as well as Salmon (v1.10.1)<sup>24</sup> for transcript-level quantification based on STAR's alignment output. To eliminate duplicate reads, the `--with_umi` option was enabled. Gene-level quantification was derived from transcript-level estimates using the R package tximport (v1.34.0)<sup>25</sup>, which sums transcript abundances for each gene. The generated raw gene-level counts were normalized and variance-stabilized using the regularized log transformation (rlog) from DESeq2 (v1.34.0)<sup>26</sup>, addressing the variance-over-mean trend. Principal component analysis (PCA) confirmed high reproducibility across biological replicates. Differential expression analysis was performed using DESeq2, identifying genes as significantly differentially expressed (DEGs) if they exhibited a fold change  $\geq 2$  and an adjusted P-value  $\leq 0.05$ . The normalized rlog-transformed counts were then used for clustering and visualization. An overrepresentation analysis of differentially expressed host genes ( $\text{padj.} \leq 0.05$  and  $\log_2\text{FC} \geq 1/\leq -1$ ) was performed with WebGestalt<sup>27</sup>. GO terms associated with biological processes were selected with an FDR  $\leq 0.05$ .

## Spatial transcriptomics experiments

SkOs were imbedded in paraffin as described for IHC staining. 3 SkOs for each condition were assembled in one agarose mold before embedding all conditions (uninfected/2dpi/3dpi/4dpi for the main experiment, uninfected/2dpi/6dpi for the pilot experiment). *In situ* RNA measurements were performed using the Xenium system (10x Genomics). The pilot experiment was done at the MDC/BIH genomics platform using nuclear expansion based on DAPI staining for cell segmentation. The main experiment was performed at the 10xGenomics facility in Stockholm using multimodal segmentation (nuclear stain, RNA and protein based cell staining, cell surface staining). For both experiments, the human multi tissue gene panel was used, supplemented by the 100 genes custom panel CZBXK3 (Table S2). Sections of 5 $\mu\text{m}$  thickness were placed on a Xenium slide according to the manufacturer's protocol, with drying at 42°C for 3 hours and overnight placement in a desiccator at room temperature, followed by deparaffinization and permeabilization to make the mRNA accessible. The Probe Hybridization Mix was prepared according to the user guide (CG000582, Rev D, 10x Genomics). The staining for Xenium was performed using Xenium Nuclei Staining Buffer (10x Genomics product number: 2000762) as a part of the Xenium Slides & Sample Prep Reagents Kit (PN-1000460). Following the Xenium run, Hematoxylin and Eosin (H&E) staining was performed on the same section according to the Post-Xenium Analyzer H&E Staining user guide (CG000613, Rev B, 10x Genomics).

## Spatial transcriptomics analysis

The spatial transcriptomics data was analyzed in R using the VoltRon package<sup>28</sup>, as well as packages from tidyverse<sup>29</sup>. Other packages used include DESeq2<sup>26</sup>, apeglm<sup>30</sup>, sf<sup>31</sup> and concaveman<sup>32</sup>. Briefly, we first assessed cell type identity only on cellular transcriptomes, i.e. without taking spatial information into account. Viral load was defined as percent viral counts (i.e., sum of the five viral genes UL54, US1, UL27, UL29, LAT) of all counts per cells. Cells with 10 or less cellular RNA counts were filtered out. Differential expression was calculated as pseudo-bulk per cell type, i.e., counts were summed up per group (0 dpi and 2 dpi all cells, 3 and 4 dpi either cells with 1 or less viral count “-”, viral load below “+”, or above the median “++” within the group). For the proximity analysis, if at least 3 cells were not more than 70  $\mu\text{m}$  apart from each other, they were taken into account (“TNF expressing”), and the proximal area defined at 280  $\mu\text{m}$  around these cells. ChatGPT (OpenAI, <https://chat.openai.com>, model o1) assisted in writing R code

## Results

### Generation of skin organoids

SkOs were produced after the protocol from Lee and colleagues<sup>19</sup> and checked for correct differentiation by brightfield microscopy, immunohistochemistry (IHC) and whole mount immunofluorescence staining (WMS) (Figure 1 and Suppl. Figure 1). The results show the expected head and tail structure with the dermis and epidermis in the head and cartilage in the tail. Our SkOs reached full complexity around 120 days after production. The hair follicles show the expected structures e.g., dermal papilla, matrix, inner root sheet, and outer root sheet (Suppl. Figure 1). We detect Merkel cells and innervation of the hair follicles with assembly of neuron somata in the organoid tail (Figure 1).

### Infection of SkOs with HSV-1

Fully differentiated SkOs (~120 days old) were infected with HSV-1 strain 17 that expresses GFP under the control of a CMV IE-promoter. Since we wanted to observe viral spread within the tissue we infected one SkO with only 800 PFU which corresponds to an approximate MOI of 0.2, when assuming  $4 \times 10^3$  cells on the organoid surface. At 2 dpi GFP expression was visible by fluorescence microscopy at spots on the surface of the organoid (Figure 2A). At 4 dpi GFP fluorescence increased and spread over the complete organoid. In IHC on sections of SkOs and WMS the infection was first detectable at sites where hair follicles protruded from the organoid surface (Figure 2B and Suppl. Figure 2). At 2 dpi the first layers of fibroblasts in the dermis showed expression of GFP, HSV-1 IE ICP0 and HSV-1 late protein gD. At 4 dpi the infection reached the inner structures of the organoid including the epidermis where the keratinocytes of the basal layer and the stratum spinosum stained positive for GFP, ICP0 and gD. Keratinocytes of the stratum corneum showed no signs of infection. Similarly, the different cell layers at the hair follicles were positive for GFP, ICP0 and gD except for the cornified hair structures. Until 8 dpi, we observed no sign of infection in these structures just as in the cartilage of the organoid tail. Furthermore, we observed a strong cytopathic effect in the infected cells. Infected fibroblasts of the dermis showed the first signs at 2 dpi and especially at 4 dpi. Infected keratinocytes in the epidermis and the inner cell layers at the hair follicles started at 6 dpi to show cytopathic effects that resulted in dissolution of the basal membrane and hair follicle integrity.

### Bulk transcriptomics of HSV-1 infected skin organoids

Having established that HSV-1 can productively infect SkOs to analyze the host response to the viral infection. We performed bulk RNA-seq of untreated and HSV-1 infected SkOs at 2, 4, 6 and 8 dpi. At 2 dpi we observed only 20 DEGs, which increased to ~1000 at 4 dpi and ~5000 at 6 and 8 dpi (Figure 3A). GO analysis of 2 dpi vs. control produced no enriched terms, due to the low number of DEGs. Analysis of 4dpi vs control showed an enrichment of GO-terms belonging to immune responses (e.g., leukocyte activation) and inflammation (e.g., response to tumor necrosis factor) in the upregulated DEGs (Figure 3 B). At 6 and 8 dpi we found terms of cellular differentiation (e.g., skin development) stand out among the downregulated DEGs. This could reflect the typical HSV-1 induced host cell shutoff<sup>33</sup>. However, the percentage of viral reads reaches ~20% of all reads already at 4dpi and increases only slightly up to ~25% at 6 and 8 dpi (Figure 3C).

### Spatial transcriptomics of HSV-1 infected skin organoids

To comprehensively understand the temporal spatial dynamics of the viral infection and the host response in the SkO model system we used spatial transcriptomics. We performed two spatial transcriptomics experiments with single cell resolution on the Xenium platform. In the

pilot experiment, we profiled sections of uninfected SkOs as well as 2 and 6 dpi. For the main experiment, we switched to 2, 3 and 4 dpi (Figure 4). We quantified expression of the ~500 measured genes, including five viral transcripts (HSV-1 US1, UL27, UL29, UL54 and LAT). Cell type identities were assigned based on non-integrated transcriptomes (Figure 4A, Suppl. Figure 3A-D). We identified all cell types, including low abundant cell types e.g., Merkel cells, that we expected to find based on single cell sequencing data and immunostainings performed by Lee and colleagues<sup>18</sup>. Furthermore, the transcriptome-based cell type assignment differentiated between subtypes that coincide with specific localization such as different fibroblasts (papillary and mesenchymal) that localize proximal or distal to the epidermis. Keratinocyte subtypes of the stratum basale, spinosum, granulosum, and corneum were distinguishable and clearly spatially restricted. Cell types of the hair follicles (dermal sheath, outer root sheath, inner root sheath, matrix, bulge region) were identified and matched their expected localization. Cell type assignments were also successful in infected SkOs (Figure 4B). However, some highly infected cells, particularly fibroblasts, lost their transcriptional identity and were thus assigned as “undefined” (Figure 4B, gray colored cells in the upper central part, and Suppl. Figure 3C). This can be visualized e.g., with complete loss of PDGFR $\alpha$  mRNA, a pan-fibroblast marker, in highly infected cells due to host cell shutoff<sup>33</sup> (compare Figure 4C and 4D, top panels). Accordingly, the proportion of “undefined” cells increased in highly infected (4dpi) vs. uninfected organoids but did not exceed ~15% of all cells (Figure 4E). When we analyzed the expression of the viral transcripts US1/ICP22, UL54/ICP27, UL29/ICP8, UL27/gB and LAT we detected, as expected from protein staining, infection starting in the outermost fibroblast layers of the dermis at 2dpi and then spread through the organoid until the infection reached the epidermis at 4dpi (Figure 4D and Suppl. Figure 3B). To investigate susceptibility and viral gene expression between the different cell types in SkOs, we first compared the proportion of infected cells in the main cell types of skin, fibroblasts and keratinocytes. We investigated the most abundant subtypes, papillary type 1 and papillary type 2 fibroblasts, as well as stratum basale and stratum spinosum keratinocytes. When looking at the percentages of cells with at least 2 viral transcript counts, papillary type 1 were more frequently infected at the earlier time points, likely due to their more exposed localization at the outside of the organoids compared to type 2 (Figure 4F, upper panel). At 4 dpi papillary fibroblasts type 1 and 2 have similar proportions of HSV-1 infected cells, in contrast to the keratinocyte populations which still have a lower proportion of positive cells. Also, the viral load remained considerably lower in keratinocytes compared to fibroblasts (Figure 4F, lower panel). Since we only measured five viral transcripts, we could not assess the entire viral gene expression cycle. We therefore focused on the immediate UL54 transcript and the very late LAT. When ordering cells along increasing viral load, we found in papillary fibroblasts the expected pattern, i.e. a strong increase of UL54 RNA at the beginning followed by a plateau/decline, with the LAT RNA constantly accumulating (Figure 4G). In stratum basale keratinocytes however, there was indication of a lag phase, and considerably slower viral replication.

Of note, particularly the stratum basale keratinocytes lie further within the tissue compared to the papillary fibroblasts, for which type 1 lies most outside and type 2 is closer to the epidermis. Since the organoids were infected from the exterior surface, the lower viral load of keratinocytes could be a consequence from them being infected at a later timepoint. We therefore investigated the relationship between distance from organoid surface and proportion of positive cells as well as viral load (Suppl. Figure S3E+F). We sorted keratinocytes of the stratum basale and papillary fibroblasts 1 and 2 into bins of equal distance to the organoid boundary and analyzed the fraction of cells with at least 2 viral counts. This showed that, even in low and medium distance to the organoid boundary, a lower proportion of keratinocytes were virus positive compared to both fibroblast subtypes. At larger distances, papillary fibroblasts type 1 also showed a lower fraction of virus positive cells than papillary type 2, which could be due to them being first infected and starting to show cytopathic effects. Interestingly, when we

analyzed the viral load in positive cells, keratinocytes of the stratum basale showed always a lower viral load than fibroblasts at the same distance to the organoid boundary. This indicates that the lower viral load in stratum basale keratinocytes compared to the main fibroblast subtypes of the dermis in SkO is not a spatial effect but rather dependent on cell type and/or extracellular structures that might restrict susceptibility and permissiveness of stratum basale keratinocytes compared to the fibroblasts in the dermis.

## Hair follicles slow down viral spread

The SkOs used here feature a multitude of structures, including hair follicles (HF) that harbor many cell types from different origins. A specific fibroblasts subtype of the dermis, the dermal sheath cells, cover the outer root sheath keratinocytes and the bulge region. At the base of HF another fibroblast subtype, the dermal papilla, are found. The inner layers of keratinocytes in HF consist of the inner root sheath and the matrix. Melanocytes can be embedded in the keratinocyte layers. When we analyzed the viral loads in the cell types of HF we found that all show considerably lower viral loads than the surrounding papillary fibroblasts with high amounts of viral RNAs (Figure 5A). Indeed, there was much less viral RNA within the hair follicles, even when the surrounding papillary fibroblasts show very high viral load (Figure 5B). Again, we analyzed if this effect was induced by the more inner localization of specific cell types, which was not the case (Suppl. Figure 4B,C). We hypothesized three potential explanations for this observation. First, there could be a layer of non-permissive cells surrounding the hair follicles. Second, a barrier of extracellular matrix might act protectively. And third, the infection cycles in the different cell types within the hair follicles could be considerably slower compared to e.g., the surrounding papillary fibroblasts.

To investigate the first possibility, we identified in organoids at 4 dpi the dermal sheath fibroblasts which surround hair follicles and are next to highly infected papillary fibroblasts (Figure 5D, Suppl. Figure S4A). Indeed, the viral load in these dermal sheath fibroblasts showed a strong drop from the cells just outside (Figure 5C). Other cell types of HF further inside showed even less viral load. Since the main spatial transcriptomics experiment only extended to 4 dpi, we went back to the immunostainings to check whether at later time points hair follicles would be fully infected, which was indeed the case (Figure 5F). So, in conclusion, the collective evidence suggests that hair follicles in general are not non-permissive, but show a much slower viral infection cycle.

## HSV-1 induces layered expression of TNF family cytokines

We next turned to investigate changes in the host transcriptome induced by the virus. HSV-1 infection leads to a general shutoff of host genome transcription<sup>33</sup> as well as read-through<sup>34</sup> and antisense transcription<sup>35</sup>, but also induction of several genes<sup>36-39</sup>. To identify host genes responding to the infection, we calculated differential expression values per cell type between infected and uninfected organoids, taking into account the viral RNA content, i.e., by separating cells into no viral RNA (less than 2 HSV-1 counts), low virus RNA (viral load below the median calculated within the cell type and time point but across all individual organoids) and high virus RNA (viral load above the median). For further analysis, we focused on the interferon-stimulated genes IRF9 and MX1, which were previously shown to be induced by viral infections of both DNA<sup>40</sup> and RNA viruses<sup>41</sup>. IRF9 mRNA was present in uninfected organoids at relatively high levels and was significantly upregulated primarily in keratinocytes of the stratum spinosum (Figure 6A, top panel). MX1 on the other side was more induced in papillary fibroblasts (Figure 6A, bottom panel). At 3dpi MX1 was significantly upregulated in subtype 1 without virus and in highly infected cells. In subtype 2 MX1 was upregulated at 4 dpi in highly infected cells. That IRF9 and MX1 were significantly upregulated also in cells without virus indicates that they were rather indirectly induced, possibly through paracrine signaling.

In our bulk RNA-seq experiment we found that genes involved in response to TNF were overrepresented in the significantly upregulated genes at 4 dpi (Figure 3B). In spatial transcriptomics, we also found the cytokines TNF (coding for TNF $\alpha$ ) and TNFSF9 (coding for 4-1BBL) significantly upregulated by HSV-1 infection. Notably, their expression was highly cell type-dependent and largely mutually exclusive, with TNF induced in keratinocytes (mainly stratum basale) and TNFSF9 in papillary fibroblasts (Figure 6B, E, F). In contrast to IRF9 and MX1, expression of TNF and TNFSF9 clearly depended on viral presence. Their expression accumulated with increasing viral load, but peaked at some point, which could be due to the shutoff of host transcription (Figure 6C and D). We verified that the signal does not originate from read-in transcription originating from HSV-1-induced disruption of transcription termination for an upstream gene<sup>34</sup>. Both the bulk RNA-seq data generated here as well as published bulk RNA-seq data from HSV-1 infected fibroblasts<sup>34</sup> and HaCat keratinocytes<sup>42</sup> did not indicate that upregulation of TNF and TNFSF9 are results of read-in. In contrast, these two datasets provided evidence from cell culture samples for TNFSF9 being induced in fibroblasts and TNF in keratinocytes. Notably, also in our SkO model we also observed in our SkO model induction of genes that results from antisense (BBC3) or read-through transcription (DUX4, CD79A, PECAM1) (Suppl. Figure S5), confirming data from HSV-1 infection of cell lines.

Taken together, we could observe localized, layered patterns of the induction of two TNF family members upon HSV-1 infection in the skin organoids. The combination of specific locations for the various cell types and cell type-dependent gene induction therefore could lead to a spatially coordinated cytokine expression upon encounter with the virus.

## Expression of TNF induces NF- $\kappa$ B targets in surrounding cells

We further investigated, if expression of TNF would lead to functional sensing in surrounding cells. We first defined cells proximal to TNF expressing cells (Figure 7A). Next, we identified potential TNF $\alpha$  induced genes in fibroblasts based on a published RNA-seq data set<sup>43</sup>. Eight of these genes were included in our spatial transcriptomics experiment (Figure 7B). By calculating the differential expression in fibroblasts proximal vs. distal to the TNF-expressing cells we found that these genes were generally upregulated proximally, however the effect was not significant in cells proximal versus distal to TNF expressing cell groups. By focusing on CXCL2, a TNF $\alpha$ -induced gene, we find a high number of cells expressing CXCL2 in the dermis close to TNF expressing keratinocytes (Figure 7C). To investigate whether this could also be caused by 4-1BBL (TNFSF9), we looked for regions with high TNFSF9 but no/low TNF expression. CXCL2 levels in these regions appeared to be considerably lower (Figure 7D). In summary, our results suggest that the cell-type specific induction of the TNF gene that leads to secretion of the TNF $\alpha$  cytokine and subsequently induction of target genes in the immediately surrounding cells.

## Discussion

In this study, we showed for the first time an infection of complex human hair bearing skin organoids with HSV-1. Due to the inside-out morphology of the organoids and the infection therefore starting from the dermis our model is closest to the reactivation scenario of HSV-1, when infectious particles are released from neuronal cells into the fibroblast layer of the dermis<sup>44</sup>. This makes our model highly relevant for investigating HSV-1 induced pathologies, since most of them are a result of reactivation and not primary infection. For instance recurrent herpes labiales has an average incidence of about 1.6 per 1000 patients each year<sup>45</sup>. Furthermore, skin organoids can also provide insights into how suppression of full lytic infections upon reactivation may be triggered<sup>46</sup>.

When analyzing the susceptibility of the cells to HSV-1 in the SkO model we found that eventually (latest time point 10 dpi) all cell types in our model system were infected by HSV-1

except for the stratum corneum, cornified structures in the HFs and cartilage in the tail of the SkO. This may be expected due to a lack of immune cells that could clear the infection. A resistance of the stratum corneum against HSV-1 infection has been reported by many other studies using mouse models and *ex vivo* skin showing that the cornified keratinocyte layer prevents HSV-1 infection by the external surface<sup>6,9</sup>. However, studies on *ex vivo* skin also showed that wounding from the external side through different approaches like microneedling lead to only limited infection of the epidermis<sup>11,12</sup>. Only infection from the dermal side by either removal of the dermis or deeper wounding through the epidermis into the dermis lead to efficient infection of the basal keratinocytes and spread to the higher differentiated keratinocyte layers<sup>9,47</sup>. This highlights the protective role of the epidermis. At the moment, we do not understand why chondrocytes are also resistant to viral infection. Since there is also no expression of the GFP reporter from the viral genome, it is likely that viral entry is already blocked. Further experiments will show if this is due to an absence of the entry receptors or simply a physical barrier by extensive extracellular matrix produced by the chondrocytes.

To understand virus spread and host response in the full complexity of our skin model system we performed spatial transcriptomics. We can clearly identify all expected cell types which allowed a cell type and location specific analysis of viral load and host response, making this a well suitable method to comprehensively study virus infections in such complex models. We identified a multitude of fibroblasts and keratinocyte subpopulations that show remarkable differences in viral loads and host responses. Viral loads in papillary fibroblasts were much higher than in keratinocytes of the stratum basale and stratum spinosum, indicating that they produce higher yield of infectious particle, thereby contributing to the rapid spread of HSV-1 through the dermis, which we observed in the SkO. However, fibroblasts of the dermal sheath and dermal papilla at HF show strongly reduced viral loads compared to adjacent papillary fibroblasts. Studies in *ex vivo* models showed that fibroblasts of the dermis are susceptible to HSV-1 although less so than keratinocytes<sup>8,11</sup>. In these studies fibroblasts were not differentiated between different subtypes. Moreover, the main subtype of adult dermis, reticular fibroblasts, is not present in our model system, which could explain the different results. In all cell types of HFs we found a delayed viral infection. Since HF are eventually infected at later time points, we exclude that entry receptors are missing on these cell types. We speculate that the delayed viral infection is a cell-type specific restriction of viral gene expression especially in cells of the dermal sheath and the dermal papilla. The keratinocyte populations of the HF could therefore be protected from viral infection or, similar to keratinocytes of the stratum basale and spinosum, in general also show a restricted viral gene expression. High resolution methods such as spatial transcriptomics will in the future allow a dissection of the dynamic of viral spread in skin.

Based on our results from bulk RNA-seq we analyzed induction of immune and inflammatory pathways, especially the TNF pathway, since this was upregulated at 4 dpi. We detected two different types of TNF cytokines being induced in infected cells, namely TNF (coding for TNF $\alpha$ ) in keratinocytes of the stratum basale express, and TNFSF9 (coding for 4-1BBL) in papillary fibroblasts. We also observed induction of TNF target genes in surrounding cells and a potential priming of adjacent uninfected cells, indicating that the gene activation is indeed functional. Induction of TNF was previously associated with HSV-1 in cerebral infections/reactivations<sup>48,49</sup>. The combination of cell-type specific TNF family inductions and the layered organization of the skin could be the onset of a spatially coordinated immune response leading to rapid suppression of reactivating virus. In the future, we want to further investigate the effect of TNF on the viral gene expression and potential protective effects on uninfected cells.

In summary, we show that SkOs are a physiologically highly relevant model system for HSV-1 infection in the skin. The combination with novel techniques that allow spatial transcriptome

analysis on the single cell level allows analysis of viral gene expression and viral host response in unprecedented depth.

## Acknowledgements

The authors thank Robert Shelansky, Aishwarya Konnur, Jana Lalakova, Morgane Rouault (10xGenomics) for performing the main spatial experiment in this manuscript and for technical support. Vera Wolf, Kathrein Permien (Charité) and Kristin Hartmann (Core Facility Experimental Histo-Pathology/UKE) provided excellent technical assistance. We thank the UKE imaging facility (umif) for excellent technical support in microscopy. We thank Claudia Schmidt, Lisann Röpke, Nina Bracker and Josephine Bonath (UKE) for excellent technical assistance in iPSCs and organoid culture.

This work was supported by the Deutsche Forschungsgemeinschaft (DFG; German Research Foundation) in the framework of the Research Unit FOR5200 DEEP-DV (443644894) project, GR 3318/5-1, LA 2941/18-1 and FI 782/7-1 to A.G., M.L. and N.F., respectively.

## References

1. James, C., Harfouche, M., Welton, N.J., Turner, K.M., Abu-Raddad, L.J., Gottlieb, S.L., and Looker, K.J. (2020). Herpes simplex virus: global infection prevalence and incidence estimates, 2016. *Bull World Health Organ* 98, 315-329. [10.2471/BLT.19.237149](https://doi.org/10.2471/BLT.19.237149).
2. Zhu, S., and Viejo-Borbolla, A. (2021). Pathogenesis and virulence of herpes simplex virus. *Virulence* 12, 2670-2702. [10.1080/21505594.2021.1982373](https://doi.org/10.1080/21505594.2021.1982373).
3. Verzosa, A.L., McGeever, L.A., Bhark, S.J., Delgado, T., Salazar, N., and Sanchez, E.L. (2021). Herpes Simplex Virus 1 Infection of Neuronal and Non-Neuronal Cells Elicits Specific Innate Immune Responses and Immune Evasion Mechanisms. *Front Immunol* 12, 644664. [10.3389/fimmu.2021.644664](https://doi.org/10.3389/fimmu.2021.644664).
4. Cunningham, A.L., Diefenbach, R.J., Miranda-Saksena, M., Bosnjak, L., Kim, M., Jones, C., and Douglas, M.W. (2006). The cycle of human herpes simplex virus infection: virus transport and immune control. *J Infect Dis* 194 Suppl 1, S11-18. [10.1086/505359](https://doi.org/10.1086/505359).
5. van Lint, A., Ayers, M., Brooks, A.G., Coles, R.M., Heath, W.R., and Carbone, F.R. (2004). Herpes simplex virus-specific CD8+ T cells can clear established lytic infections from skin and nerves and can partially limit the early spread of virus after cutaneous inoculation. *J Immunol* 172, 392-397. [10.4049/jimmunol.172.1.392](https://doi.org/10.4049/jimmunol.172.1.392).
6. Kollias, C.M., Huneke, R.B., Wigdahl, B., and Jennings, S.R. (2015). Animal models of herpes simplex virus immunity and pathogenesis. *J Neurovirol* 21, 8-23. [10.1007/s13365-014-0302-2](https://doi.org/10.1007/s13365-014-0302-2).
7. Silva, J.R., Lopes, A.H., Talbot, J., Cecilio, N.T., Rossato, M.F., Silva, R.L., Souza, G.R., Silva, C.R., Lucas, G., Fonseca, B.A., et al. (2017). Neuroimmune-Glia Interactions in the Sensory Ganglia Account for the Development of Acute Herpetic Neuralgia. *J Neurosci* 37, 6408-6422. [10.1523/JNEUROSCI.2233-16.2017](https://doi.org/10.1523/JNEUROSCI.2233-16.2017).
8. Wirtz, L., De La Cruz, N.C., Mockel, M., and Knebel-Morsdorf, D. (2022). Susceptibility of Human and Murine Dermal Fibroblasts to Herpes Simplex Virus 1 in the Absence and Presence of Extracellular Matrix. *J Virol* 96, e0206821. [10.1128/JVI.02068-21](https://doi.org/10.1128/JVI.02068-21).
9. Rahn, E., Petermann, P., Thier, K., Bloch, W., Morgner, J., Wickstrom, S.A., and Knebel-Morsdorf, D. (2015). Invasion of Herpes Simplex Virus Type 1 into Murine Epidermis: An Ex Vivo Infection Study. *J Invest Dermatol* 135, 3009-3016. [10.1038/jid.2015.290](https://doi.org/10.1038/jid.2015.290).
10. Wirtz, L., Mockel, M., and Knebel-Morsdorf, D. (2020). Invasion of Herpes Simplex Virus 1 into Murine Dermis: Role of Nectin-1 and Herpesvirus Entry Mediator as Cellular Receptors during Aging. *J Virol* 94. [10.1128/JVI.02046-19](https://doi.org/10.1128/JVI.02046-19).
11. De La Cruz, N.C., Mockel, M., Wirtz, L., Sunaoglu, K., Malter, W., Zinser, M., and Knebel-Morsdorf, D. (2021). Ex Vivo Infection of Human Skin with Herpes Simplex Virus 1 Reveals Mechanical Wounds as Insufficient Entry Portals via the Skin Surface. *J Virol* 95, e0133821. [10.1128/JVI.01338-21](https://doi.org/10.1128/JVI.01338-21).

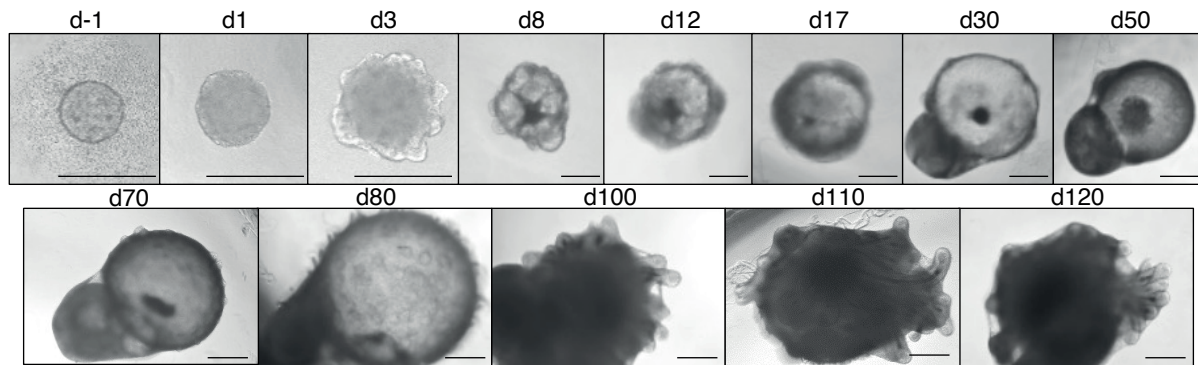
12. Tajpara, P., Mildner, M., Schmidt, R., Vierhapper, M., Matiasek, J., Popow-Kraupp, T., Schuster, C., and Elbe-Burger, A. (2019). A Preclinical Model for Studying Herpes Simplex Virus Infection. *J Invest Dermatol* 139, 673-682. 10.1016/j.jid.2018.08.034.
13. Sun, S., Jin, L., Zheng, Y., and Zhu, J. (2022). Modeling human HSV infection via a vascularized immune-competent skin-on-chip platform. *Nat Commun* 13, 5481. 10.1038/s41467-022-33114-1.
14. Andrei, G., van den Oord, J., Fiten, P., Opdenakker, G., De Wolf-Peeters, C., De Clercq, E., and Snoeck, R. (2005). Organotypic epithelial raft cultures as a model for evaluating compounds against alphaherpesviruses. *Antimicrob Agents Chemother* 49, 4671-4680. 10.1128/AAC.49.11.4671-4680.2005.
15. Chu, J.T.S., and Lamers, M.M. (2024). Organoids in virology. *npj Viruses* 2, 5. 10.1038/s44298-024-00017-5.
16. Su, X., Yue, P., Kong, J., Xu, X., Zhang, Y., Cao, W., Fan, Y., Liu, M., Chen, J., Liu, A., and Bao, F. (2021). Human Brain Organoids as an In Vitro Model System of Viral Infectious Diseases. *Front Immunol* 12, 792316. 10.3389/fimmu.2021.792316.
17. Shen, Q., Zhou, Y.H., and Zhou, Y.Q. (2024). A prospects tool in virus research: Analyzing the applications of organoids in virus studies. *Acta Trop* 254, 107182. 10.1016/j.actatropica.2024.107182.
18. Lee, J., Rabbani, C.C., Gao, H., Steinhart, M.R., Woodruff, B.M., Pflum, Z.E., Kim, A., Heller, S., Liu, Y., Shipchandler, T.Z., and Koehler, K.R. (2020). Hair-bearing human skin generated entirely from pluripotent stem cells. *Nature* 582, 399-404. 10.1038/s41586-020-2352-3.
19. Lee, J., van der Valk, W.H., Serdy, S.A., Deakin, C., Kim, J., Le, A.P., and Koehler, K.R. (2022). Generation and characterization of hair-bearing skin organoids from human pluripotent stem cells. *Nat Protoc* 17, 1266-1305. 10.1038/s41596-022-00681-y.
20. Hafezi, W., Lorentzen, E.U., Eing, B.R., Muller, M., King, N.J., Klupp, B., Mettenleiter, T.C., and Kuhn, J.E. (2012). Entry of herpes simplex virus type 1 (HSV-1) into the distal axons of trigeminal neurons favors the onset of nonproductive, silent infection. *PLoS Pathog* 8, e1002679. 10.1371/journal.ppat.1002679.
21. Ewels, P.A., Peltzer, A., Fillinger, S., Patel, H., Alneberg, J., Wilm, A., Garcia, M.U., Di Tommaso, P., and Nahnsen, S. (2020). The nf-core framework for community-curated bioinformatics pipelines. *Nat Biotechnol* 38, 276-278. 10.1038/s41587-020-0439-x.
22. Di Tommaso, P., Chatzou, M., Floden, E.W., Barja, P.P., Palumbo, E., and Notredame, C. (2017). Nextflow enables reproducible computational workflows. *Nat Biotechnol* 35, 316-319. 10.1038/nbt.3820.
23. Dobin, A., Davis, C.A., Schlesinger, F., Drenkow, J., Zaleski, C., Jha, S., Batut, P., Chaisson, M., and Gingeras, T.R. (2013). STAR: ultrafast universal RNA-seq aligner. *Bioinformatics* 29, 15-21. 10.1093/bioinformatics/bts635.
24. Patro, R., Duggal, G., Love, M.I., Irizarry, R.A., and Kingsford, C. (2017). Salmon provides fast and bias-aware quantification of transcript expression. *Nat Methods* 14, 417-419. 10.1038/nmeth.4197.
25. Sonesson, C., Love, M., and Robinson, M. (2015). Differential analyses for RNA-seq: transcript-level estimates improve gene-level inferences [version 1; peer review: 2 approved]. *F1000Research* 4. 10.12688/f1000research.7563.1.
26. Love, M.I., Huber, W., and Anders, S. (2014). Moderated estimation of fold change and dispersion for RNA-seq data with DESeq2. *Genome Biol* 15, 550. 10.1186/s13059-014-0550-8.
27. Elizarraras, J.M., Liao, Y., Shi, Z., Zhu, Q., Pico, A.R., and Zhang, B. (2024). WebGestalt 2024: faster gene set analysis and new support for metabolomics and multi-omics. *Nucleic Acids Res* 52, W415-W421. 10.1093/nar/gkae456.
28. Manukyan, A., Bahry, E., Wyler, E., Becher, E., Pascual-Reguant, A., Plumbom, I., Dikmen, H.O., Elezkurtaj, S., Conrad, T., Altmüller, J., et al. (2023). VoltRon: A Spatial

- Omics Analysis Platform for Multi-Resolution and Multi-omics Integration using Image Registration. *bioRxiv*, 2023.2012.2015.571667. 10.1101/2023.12.15.571667.
29. Wickham, H., Averick, M., Bryan, J., Chang, W., McGowan, L.D.a., François, R., Golemund, G., Hayes, A., Henry, L., Hester, J., et al. (2019). Welcome to the Tidyverse. *Journal of Open Source Software* 4, 1686. 10.21105/joss.01686.
  30. Zhu, A., Ibrahim, J.G., and Love, M.I. (2019). Heavy-tailed prior distributions for sequence count data: removing the noise and preserving large differences. *Bioinformatics* 35, 2084-2092. 10.1093/bioinformatics/bty895.
  31. Pebesma, E. (2018). Simple Features for R: Standardized Support for Spatial Vector Data. *The R Journal* 10, 439-446. 10.32614/RJ-2018-009.
  32. Gombin, J., Vaidyanathan, R., and Agafonkin, V. (2020). concaveman: A Very Fast 2D Concave Hull Algorithm.
  33. Hennig, T., Djakovic, L., Dolken, L., and Whisnant, A.W. (2021). A Review of the Multipronged Attack of Herpes Simplex Virus 1 on the Host Transcriptional Machinery. *Viruses* 13. 10.3390/v13091836.
  34. Rutkowski, A.J., Erhard, F., L'Hernault, A., Bonfert, T., Schilhabel, M., Crump, C., Rosenstiel, P., Efstathiou, S., Zimmer, R., Friedel, C.C., and Dolken, L. (2015). Widespread disruption of host transcription termination in HSV-1 infection. *Nat Commun* 6, 7126. 10.1038/ncomms8126.
  35. Wyler, E., Menegatti, J., Franke, V., Kocks, C., Boltengagen, A., Hennig, T., Theil, K., Rutkowski, A., Ferrai, C., Baer, L., et al. (2017). Widespread activation of antisense transcription of the host genome during herpes simplex virus 1 infection. *Genome Biol* 18, 209. 10.1186/s13059-017-1329-5.
  36. Full, F., van Gent, M., Sparrer, K.M.J., Chiang, C., Zurenski, M.A., Scherer, M., Brockmeyer, N.H., Heinzerling, L., Sturzl, M., Korn, K., et al. (2019). Centrosomal protein TRIM43 restricts herpesvirus infection by regulating nuclear lamina integrity. *Nat Microbiol* 4, 164-176. 10.1038/s41564-018-0285-5.
  37. Wyler, E., Franke, V., Menegatti, J., Kocks, C., Boltengagen, A., Praktijnjo, S., Walch-Ruckheim, B., Bosse, J., Rajewsky, N., Grasser, F., et al. (2019). Single-cell RNA-sequencing of herpes simplex virus 1-infected cells connects NRF2 activation to an antiviral program. *Nat Commun* 10, 4878. 10.1038/s41467-019-12894-z.
  38. Full, F., Walter, S., Neugebauer, E., Tan, J., Drayman, N., Franke, V., Tay, S., Landthaler, M., Akalin, A., Ensser, A., and Wyler, E. (2023). Herpesviruses mimic zygotic genome activation to promote viral replication. *Res Sq.* 10.21203/rs.3.rs-3125635/v1.
  39. Neugebauer, E., Walter, S., Tan, J., Drayman, N., Franke, V., van Gent, M., Pennisi, S., Veratti, P., Stein, K.S., Welker, I., et al. (2025). Herpesviruses mimic zygotic genome activation to promote viral replication. *Nat Commun* 16, 710. 10.1038/s41467-025-55928-5.
  40. Gonzalez-Perez, A.C., Stempel, M., Wyler, E., Urban, C., Piras, A., Hennig, T., Ganskih, S., Wei, Y., Heim, A., Landthaler, M., et al. (2021). The Zinc Finger Antiviral Protein ZAP Restricts Human Cytomegalovirus and Selectively Binds and Destabilizes Viral UL4/UL5 Transcripts. *mBio* 12. 10.1128/mBio.02683-20.
  41. Hofmann, N., Bartkuhn, M., Becker, S., Biedenkopf, N., Bottcher-Friebertshauer, E., Brinkrolf, K., Dietzel, E., Fehling, S.K., Goesmann, A., Heindl, M.R., et al. (2024). Distinct negative-sense RNA viruses induce a common set of transcripts encoding proteins forming an extensive network. *J Virol* 98, e0093524. 10.1128/jvi.00935-24.
  42. Chopra, S., Roesner, L.M., Döhner, K., Zeitvogel, J., Traidl, S., Rodriguez, E., Harder, I., Lieb, W., Weidinger, S., Schulz, T.F., et al. (2024). Identification and characterization of collagen XXIII alpha 1 as a novel risk factor for eczema herpeticum. *medRxiv*, 2024.2007.2013.24310236. 10.1101/2024.07.13.24310236.
  43. Jones, K., Ramirez-Perez, S., Niu, S., Gangishetti, U., Drissi, H., and Bhattaram, P. (2022). SOX4 and RELA Function as Transcriptional Partners to Regulate the Expression

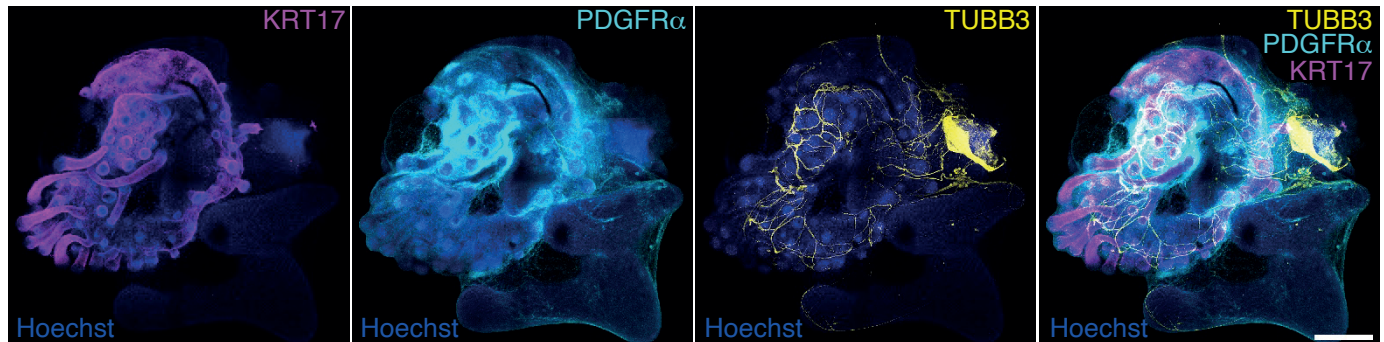
- of TNF- Responsive Genes in Fibroblast-Like Synoviocytes. *Front Immunol* 13, 789349. 10.3389/fimmu.2022.789349.
44. Bai, L., Xu, J., Zeng, L., Zhang, L., and Zhou, F. (2024). A review of HSV pathogenesis, vaccine development, and advanced applications. *Mol Biomed* 5, 35. 10.1186/s43556-024-00199-7.
  45. Gopinath, D., Koe, K.H., Maharajan, M.K., and Panda, S. (2023). A Comprehensive Overview of Epidemiology, Pathogenesis and the Management of Herpes Labialis. *Viruses* 15. 10.3390/v15010225.
  46. Roychoudhury, P., Swan, D.A., Duke, E., Corey, L., Zhu, J., Dave, V., Spuhler, L.R., Lund, J.M., Prlic, M., and Schiffer, J.T. (2020). Tissue-resident T cell-derived cytokines eliminate herpes simplex virus-2-infected cells. *J Clin Invest* 130, 2903-2919. 10.1172/JCI132583.
  47. Petermann, P., Thier, K., Rahn, E., Rixon, F.J., Bloch, W., Ozcelik, S., Krummenacher, C., Barron, M.J., Dixon, M.J., Scheu, S., et al. (2015). Entry mechanisms of herpes simplex virus 1 into murine epidermis: involvement of nectin-1 and herpesvirus entry mediator as cellular receptors. *J Virol* 89, 262-274. 10.1128/JVI.02917-14.
  48. Mancini, M., and Vidal, S.M. (2018). Insights into the pathogenesis of herpes simplex encephalitis from mouse models. *Mamm Genome* 29, 425-445. 10.1007/s00335-018-9772-5.
  49. Rybak-Wolf, A., Wyler, E., Pentimalli, T.M., Legnini, I., Oliveras Martinez, A., Glazar, P., Loewa, A., Kim, S.J., Kaufer, B.B., Woehler, A., et al. (2023). Modelling viral encephalitis caused by herpes simplex virus 1 infection in cerebral organoids. *Nat Microbiol* 8, 1252-1266. 10.1038/s41564-023-01405-y.

Figure 1

A



B



C

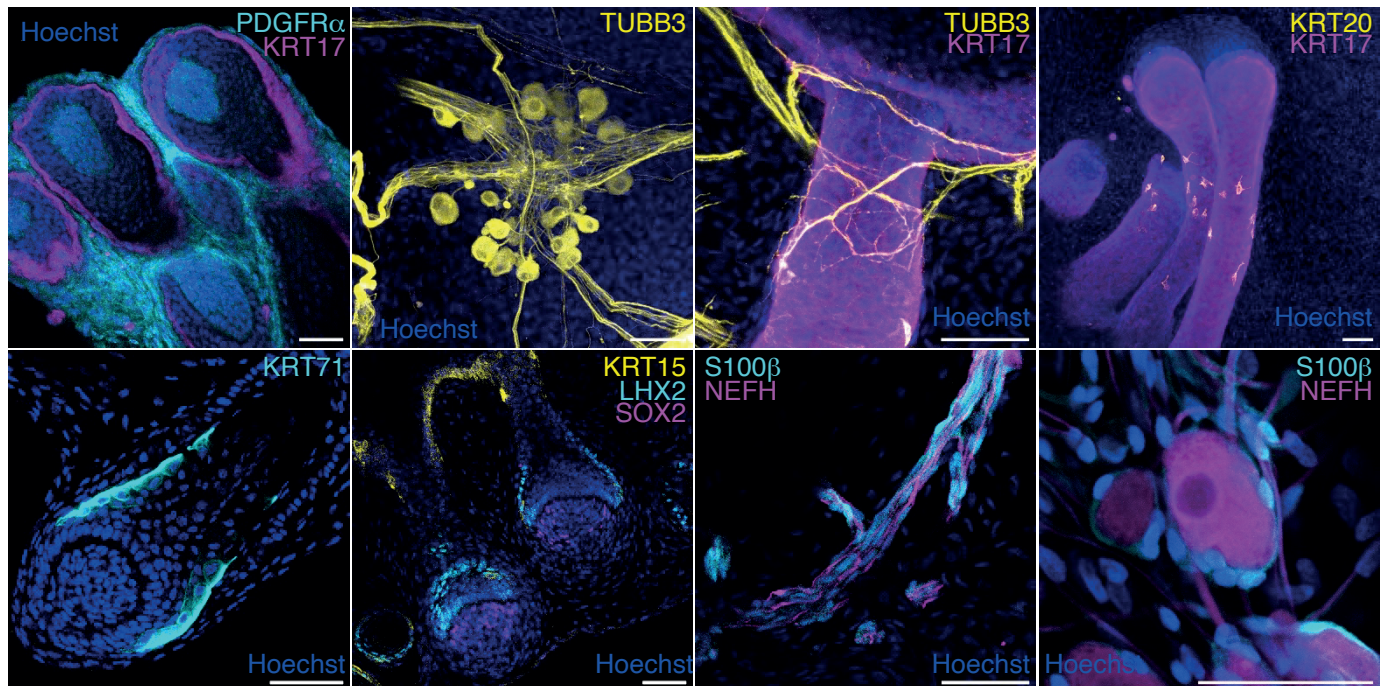


**Figure 1: Characterization of SkO differentiation.** **A**, Brightfield images of SkO from -1 (d-1) to 120 days (d120) of differentiation. Scale bars 500 $\mu$ m. **B**, Maximum intensity projections from Z-stack overview images of whole mount IF staining of 120 days old SkOs. Scale bar 500 $\mu$ m. **C**, Zoom-ins of whole mount IF staining. Scale bars 50 $\mu$ m. **C**, Zoom-ins of whole mount IF staining. Scale bars 50 $\mu$ m. KRT17: Epidermis, outer root sheath of hair. PDGFR $\alpha$ : Dermal fibroblasts, dermal papilla. TUBB3: Neuronal cells, Schwann cells. Hoechst: Nuclear stain. KRT20: Merkel cells. KRT71: Inner root sheath of hair. KRT15: basal layer of epidermis, outer root sheath, medulla. LHX2: Bulge region, hair germs, hair pegs, hair placodes. SOX2: Dermal condensates, dermal papilla, melanocytes, Merkel cells. S100 $\beta$ : Schwann cells, satellite glial cells. NEFH: Sensory neurons, large soma neurons.

Figure 2

**Figure 2: Infection of SkOs with HSV-1 leads to cytopathic effects.** **A**, Brightfield (BF) and fluorescence (GFP) images of 120 days old SkO untreated and infected with HSV-1 (expressing GFP from CMV promoter) at 2, 4, 6, and 8 days post infection (dpi). Scale bars 500 $\mu$ m. **B**, IHC staining of 120 days old SkO infected with HSV-1. Arrows in overview images indicate areas of higher magnification shown below. Time points as in A. Scale bars 500 $\mu$ m in overview images and 20 $\mu$ m in zoom-ins. Upper picture of zoom-ins shows always left epidermis and right dermis with basal layer in the middle. Lower picture in zoom-ins shows hair follicle. H&E: Hematoxylin and eosin stain. GFP: Staining against GFP expressed by HSV-1 from CMV promoter. gD: Staining against HSV-1 glycoprotein D.

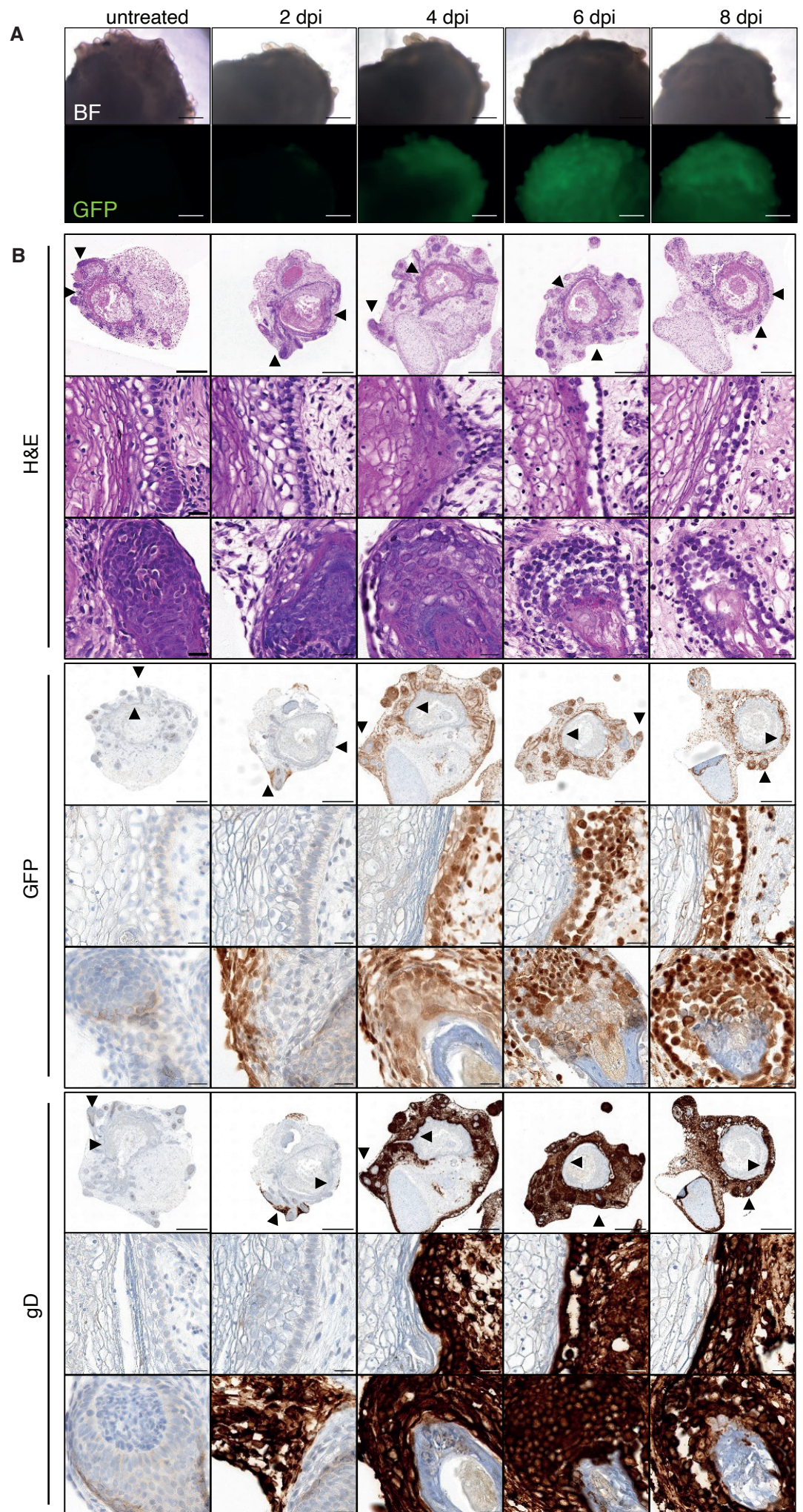


Figure 3

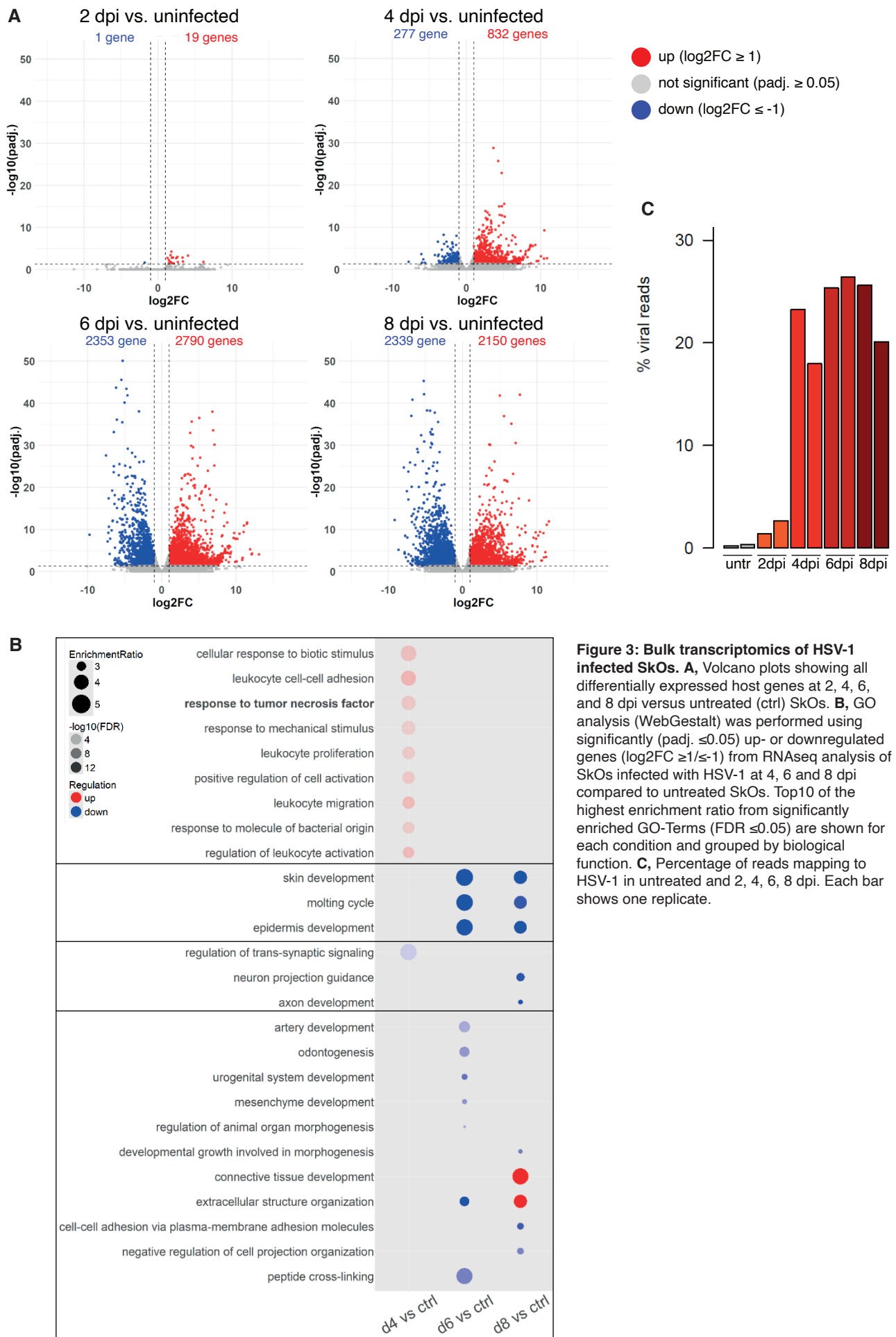
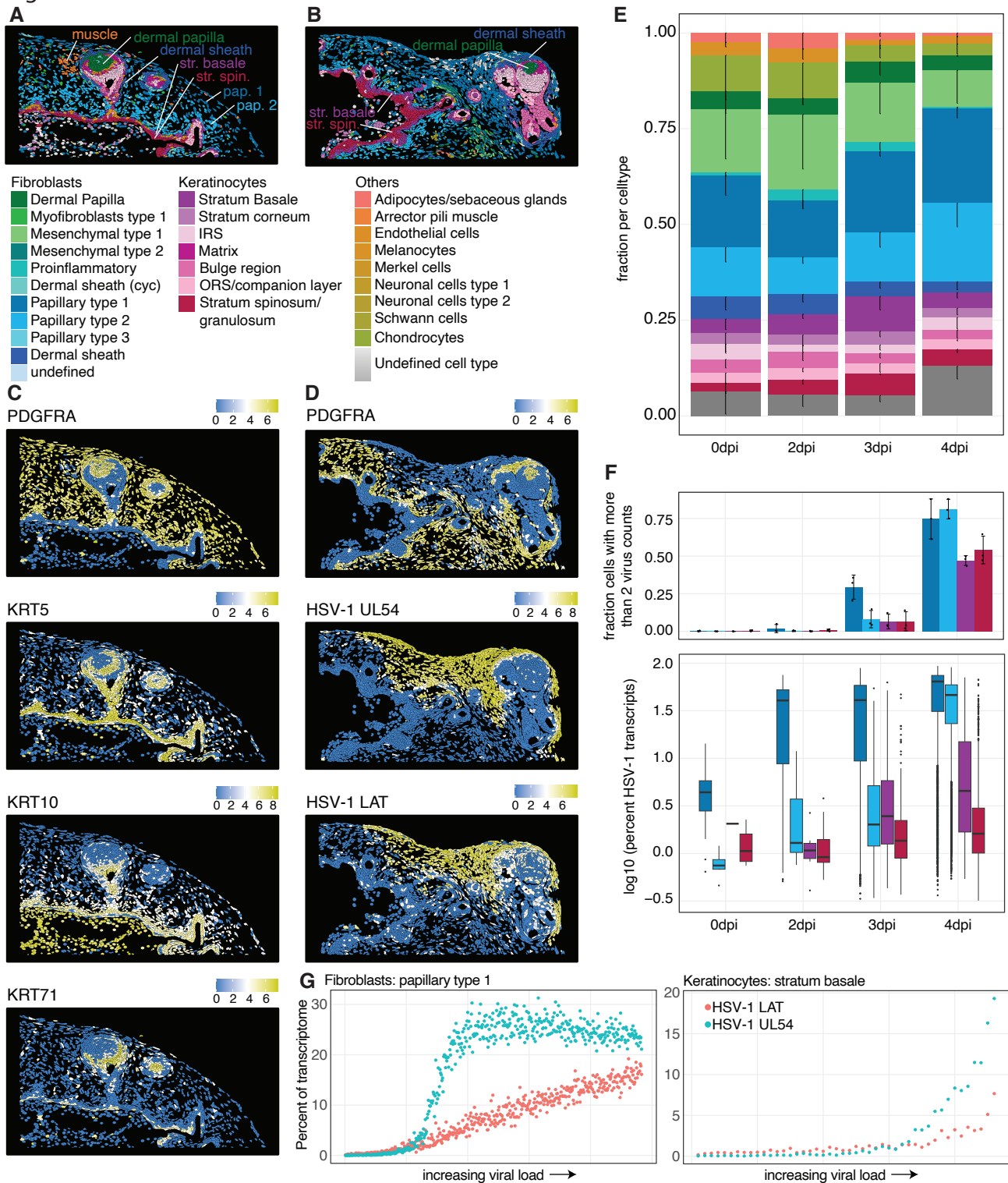
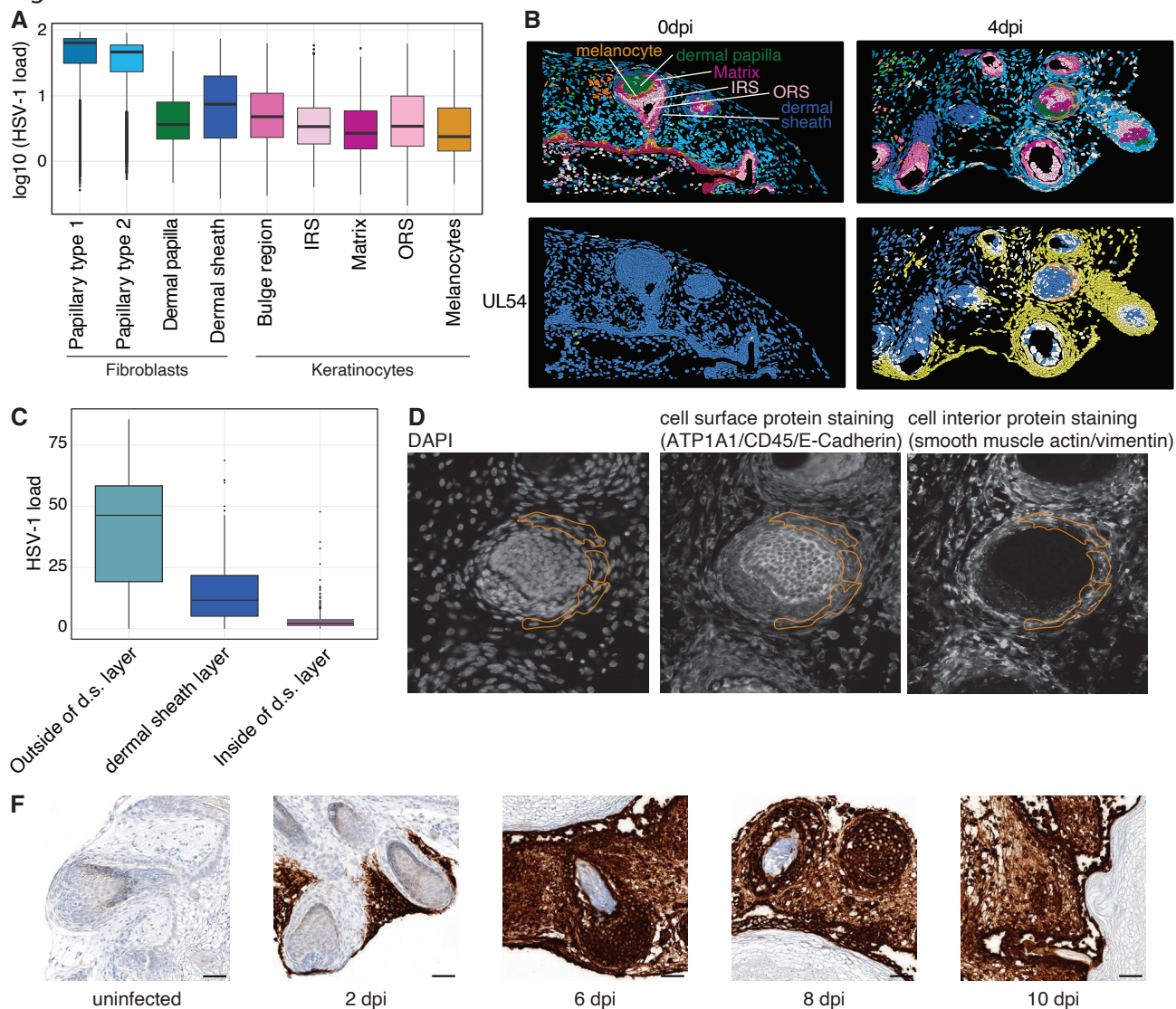


Figure 4



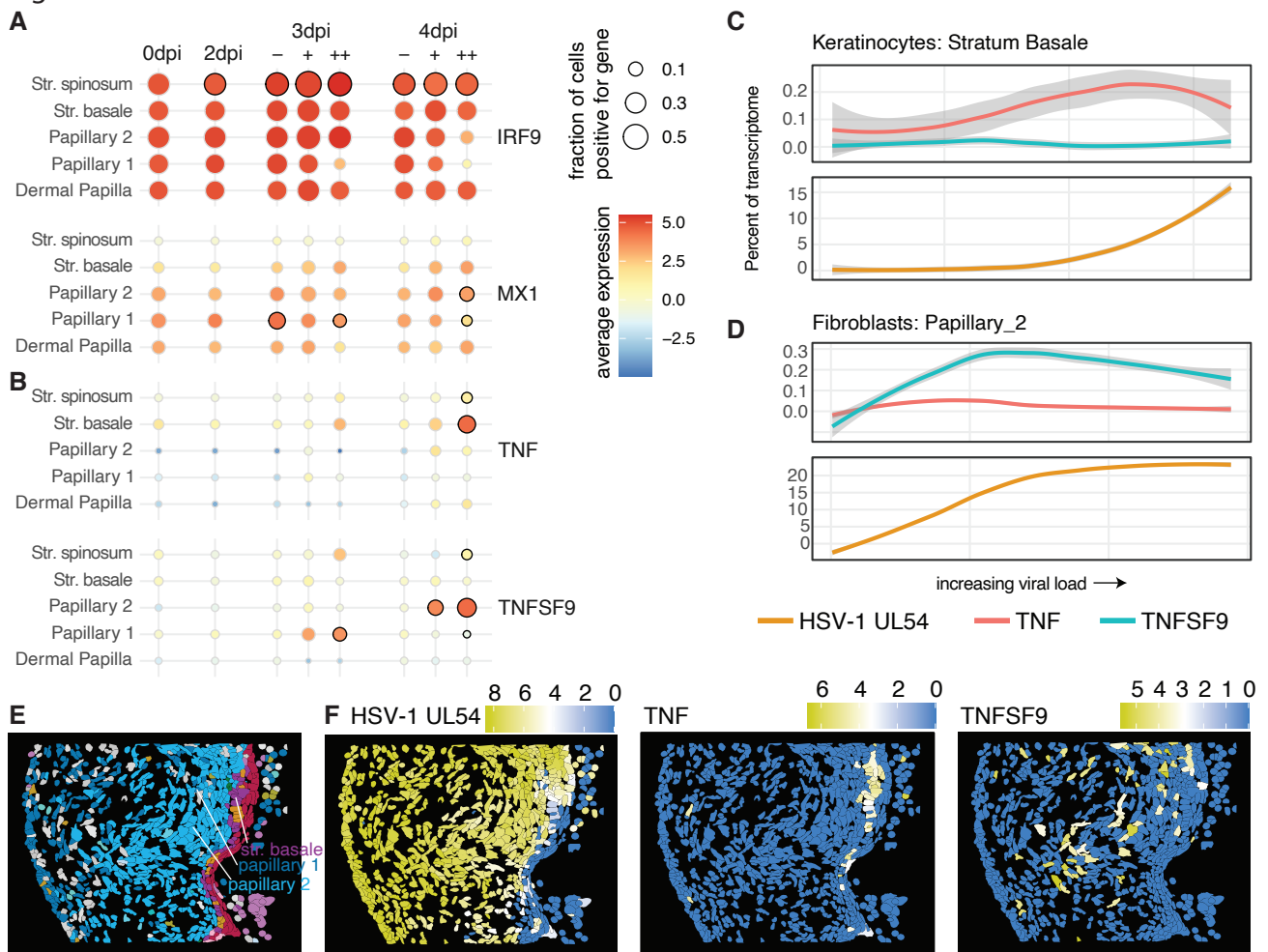
**Figure 4: Spatial transcriptomics of HSV-1 infected skin organoids.** **AB**, shown is a part of an uninfected (A) organoid and one at 3dpi, with cells colored by cell type. **CD**, the same sections as in **AB**, but colored by expression levels of the indicated genes. **E**, relative abundances of selected cell types at the different time-points. Thin lines represent standard deviations across the three organoids per timepoint. Coloring as in **AB**. **F**, upper part, percent of cells with at least 2 HSV-1 transcript counts for selected cell types. Indicated are individual values from the three organoids per timepoint, and standard deviations. Lower part, distribution of log10-transformed viral loads (percent viral transcripts). The middle line in the boxplot displays the median, the box indicates the first and third quartile, whiskers the 1.5 interquartile range (IQR). Outliers beyond are marked by single dots. **G**, cells with at least 2 viral counts were ordered along viral load and binned with 20 cells per bin. Shown are the percentages of the two indicated viral transcripts within the bin for papillary type 1 fibroblasts (left) and stratum basale keratinocytes (right).

Figure 5



**Figure 5: Hair follicles show higher resistance to virus infection.** **A**, viral load of the celltypes present in hair follicles, in comparison to type 1/2 papillary fibroblasts. **B**, HSV-1 UL54 expression around hair follicles. Shown are two segments from an uninfected organoids (left) and a 4dpi organoid (right). Top row: cells colored by celltype, with hair follicle cell types labeled. Bottom row: cells colored by normalized HSV-1 UL54 expression. Surrounded with orange are dermal sheaths in proximity to highly infected papillary fibroblasts. **C**, dermal sheath cells were identified by being next to cells with more than 20% viral load. Their viral load (middle box) is shown next to the viral load of cells not more than 50 micrometers outside of the hair follicle (left box) or 50 micrometers inside the hair follicle (right box). **D**, DAPI, cell surface protein and interior protein staining on the Xenium slide. Surrounded with orange blue are dermal sheath cells as in B. **E**, Slices of infected organoids harvested at the indicated timepoints post infection were stained using immunohistochemistry against the viral gD protein.

Figure 6



**Figure 6: Celltype-specific induction of cytokines.** **AB**, expression values of the indicated genes in a subset of cell types. For uninfected and 2dpi organoids, all cells are aggregated. For 3dpi and 4dpi, cells are split up in those with no or only 1 viral count (-), and those with viral load below (+) and above (++) the median, with the median viral load calculated only within cells with more than 1 counts. Dot sizes represent the fraction of cells having at least one count of the specified gene, the color the average expression. If the dot is encircled in black, this indicates significant different expression in a pseudobulk comparison vs. all cells in uninfected cells. **CD**, cells with at least 2 viral counts were ordered along viral load and binned with 20 cells per bin. Shown are the percentages of TNF, TNFSF9 and HSV-1 UL54 within the bin for stratum basale keratinocytes (B) and papillary 1 fibroblasts (C). **EF**, shown is a part of an uninfected SkO at 4dpi, with cells colored by cell type (E) or colored by expression levels of the indicated genes (F).

